Dynamics of the Active Loop of Snake Toxins As Probed by Time-Resolved Polarized Tryptophan Fluorescence†

P. Blandin,‡ F. Mérola,*,‡ J. C. Brochon,‡ O. Trémeau,§ and A. Ménez§

Laboratoire pour l'Utilisation du Rayonnement Electromagnétique (LURE), Centre Universitaire Paris-Sud, CNRS-CEA-MEN Bat209D, F91405 Orsay, France, and Département d'Ingénierie et d'Etude des Protéines, Commissariat à l'Energie Atomique (CEA) Saclay, F91191 Gif-sur-Yvette, France

Received May 18, 1993; Revised Manuscript Received December 20, 1993®

ABSTRACT: The local environment and dynamics of the single tryptophan residue in the respective active loops of cardiotoxin and α-neurotoxin from *Naja nigricollis* and of erabutoxin *b* from *Laticauda semifasciata* have been studied by steady-state and time-resolved polarized fluorescence and analyzed with distributions of decay times. Trp11 in loop I of cardiotoxin exhibits a very broad and complex distribution of fluorescence lifetimes at 20 °C. Despite its relatively external location in the toxin, the residue appears to be partly shielded from water and shows restricted but significant conformational fluctuations on the picosecond and nanosecond time scales. The thermal stability of cardiotoxin allowed a study of its static and dynamic fluorescence properties over a large range of temperatures. Interconversions in the intermediate nanosecond range lead to a thorough reorganization of the cardiotoxin fluorescence lifetime distribution with temperature. On the contrary, the fluorescence kinetics of Trp29 in loop II of the two neurotoxins is dominated by about 80% of a major decay time, which suggests that a nearly unique local conformation of the toxin is maintained over all time scales above the sub-nanosecond range. The fluorescence anisotropy decays show that the residue also has extremely limited rotational freedom down to the picosecond time scale. These findings are in good agreement with structural and dynamic information previously reported on the different toxins from NMR and X-ray crystallographic studies. The different dynamic properties around the tryptophan residue of the cardiotoxin and neurotoxin active loops can be analyzed within the frame of their different respective mechanisms of toxicity.

Understanding the lethal action of snake venom not only should help in protecting humans against it but may also contribute valuable information on widespread and vital biological functions. Snake venoms are complex protein mixtures with activities optimized for the efficient seizure and digestion of the specific prey of a given snake species. Cardiotoxins and neurotoxins are the major lethal components of cobra venoms (Fryklund & Eacker, 1975; Bougis et al., 1986). They share homologous amino acid sequences with a large number of basic residues and strikingly similar topologies (Figure 1). The respective crystallographic and NMR solution structures of cardiotoxins and short neurotoxins (Bourne et al., 1985; Steinmetz et al., 1988; Rees et al., 1987; Zinn-Justin et al., 1992; Gilquin et al., 1993) show flat, slightly concave molecules consisting of three loops rich in β-sheet protruding out of a core of four disulfide bridges. However, cardiotoxins and neurotoxins are responsible for very different physiological effects.

The short neurotoxins belong to the well-known family of postsynaptic curaremimetic toxins (Endo & Tamiya, 1991). These toxins block neuromuscular transmission by selectively binding to the acetylcholine receptor (AcChoR). The functionally important residues of these toxins have been located mostly on loops II and III. They form a well-defined conserved region on the concave side of the molecule, including Lys27, Trp29, Asp31, a hydrophobic residue in position 32, Arg33, and Lys- or Arg47 (Figure 1).

Cardiotoxin shows no affinity for AcChoR, but was identified as the fraction responsible for the specific ability of cobra venoms to provoke systolic cardiac arrest. More generally, it has been shown to act as a depolarizing and lytic factor on a wide variety of cells (Dufton & Hider, 1988). Contrary to the neurotoxins, the exact target and mode of action of cardiotoxins at a molecular level are still controversial, although an interaction with negatively charged phospholipids (Dufourcq & Faucon, 1978; Vincent et al., 1978) is currently the preferred initial step, followed by severe perturbations of the cell membrane (Désormeaux et al., 1992). Several studies have repeatedly pointed to the prime role of the conserved hydrophobic loop I in these interactions (Dufourcq et al., 1982; Bougis et al., 1983; Marchot et al., 1988; Ménez et al., 1990), and more specifically to Lys12 (Gatineau et al., 1990) and Trp11 (Gatineau et al., 1987). A putative phospholipid binding site has also been proposed recently on the basis of the crystal and solution structures of cardiotoxin (Gilquin et al., 1993).

Thus, cardiotoxins and curaremimetic toxins have, within a similar overall three-dimensional structure, a differently located functional site, within which is found, in most cases, a single tryptophan residue. This study aims at investigating these sites through the intrinsic spectroscopic properties of the indole side chain in, respectively, cardiotoxin and α-neurotoxin from the spitting cobra *Naja nigricollis* and erabutoxin *b*, a homologous short neurotoxin from the sea snake *Laticauda semifasciata*. In keeping with the different locations of the tryptophan residue, we found that the fluorescence of cardiotoxin differs notably from that of the two neurotoxins. In cardiotoxin, conformational fluctuations of side chains in the active loop produce an extremely heterogeneous fluorescence signal. On the contrary, the tryptophan residue of the two neurotoxins was found to be rigidly held in the protein ma-

† This work was supported by the Centre National de la Recherche Scientifique, the Commissariat à l'Energie Atomique, and the Ministère de l'Education Nationale. P.B. was supported by a grant from the CNRS.

* Author to whom correspondence should be adressed.
‡ Université Paris-Sud.
§ CEA Saclay.

® Abstract published in *Advance ACS Abstracts,* February 15, 1994.

0006-2960/94/0433-2610$04.50/0

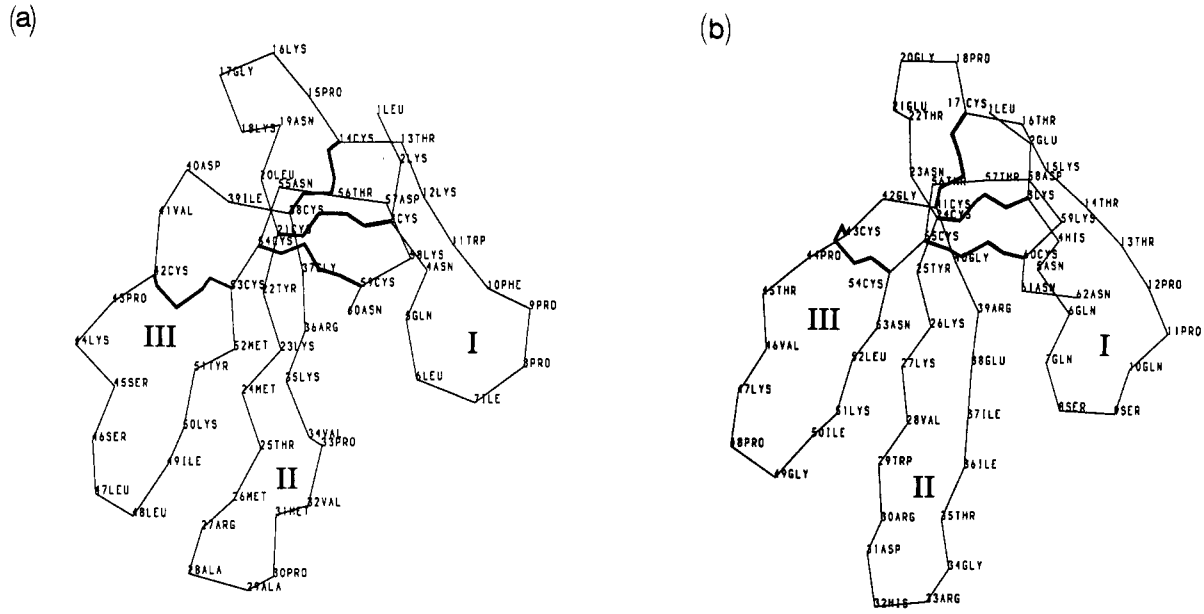

(c)

	0	10	20	30
α-neurotoxin:	L E C H N Q Q S S Q P P T T K T C P _ G E T N C Y K K V W R D H R G T I I E R			
erabutoxin b:	R I C F N H Q S S Q P Q T T K T C S P G E S S C Y H K Q W S D F R G T I I E R			

	40	50	60
	G C G C P T V K P G I K L N C C T T D K C N N		
	G C G C P T V K P G I K L S C C E S E V C N N		

FIGURE 1: Schematic diagrams of main-chain folding along α-carbons of (a) cardiotoxins and (b) short neurotoxins after the respective NMR solution structures of *N. nigricollis* cardiotoxin (Gilquin et al., 1993) and α-neurotoxin (Zinn-Justin et al., 1992). (c) Aligned sequences of *N. nigricollis* α-neurotoxin and *L. semifasciata* erabutoxin *b*. A blank residue is inserted at position 19 of the α-neurotoxin sequence to fit the numbering of erabutoxin residues (Endo & Tamiya, 1991).

trix and showed very similar and simple fluorescence kinetics in both toxins. Some degree of internal flexibility might be useful in the structural adaptation of cardiotoxin during its transfer from an aqueous environment to a membrane interface. For curaremimetic neurotoxins, the precise conservation throughout species of the local three-dimensional structure of the active loop, on one hand, and the great rigidity of this region, on the other hand, are perhaps important for effective recognition and blocking of the cholinergic receptor.

EXPERIMENTAL PROCEDURES

Materials. Cardiotoxin and α-neurotoxin from *Naja Nigricollis* and erabutoxin *b* from *Laticauda semifasciata* were isolated from the total venoms (Pasteur Institute, Paris), as previously described (Grognet, 1988; Frycklund & Eacker, 1975). After this procedure, the fluorescence anisotropy decays of cardiotoxin indicated the presence of significant amounts of aggregates, which were completely removed by additional reverse-phase HPLC (Mérola et al., manuscript in preparation). In the present article, all cardiotoxin samples were submitted to this HPLC treatment (Gatineau et al., 1990), leading to the pure monomer.

All experiments were carried out in a 10 mM cacodylate buffer, 1 mM NaCl, 0.1 mM EDTA (pH 7.0). Protein concentrations were in the ranges 40–60 μM for the steady-state fluorescence measurements and 80–90 μM for the time-resolved measurements. *N*-Acetyltryptophanamide (NATA) was from Sigma and was used without further purification. Other chemicals were of the highest grade available from Merck.

Steady-State Fluorescence. The fluorescence emission spectra were recorded on aliquots with OD values near 0.1 at the excitation wavelength, on a modified SLM 8000 spectrofluorometer, and corrected for fluctuations in excitation intensity by the signal of a rhodamine quantum counter. The excitation polarizer was set to the vertical position, and the fluorescence spectra were recorded with the emission polarizer also set to the vertical position to avoid Wood's anomaly of the emission grating. After subtraction of the Raman signal of the buffer, $R(\lambda)$, the approximate quantum yields were computed by comparison with the fluorescence, $N(\lambda)$, of NATA, from integrals of uncorrected spectra, and expressed in wavelength units. Since the spectra were measured along I_{vv}, a correction factor was introduced to account for the polarization of protein fluorescence:

$$\Phi_f = \Phi_f(\mathrm{NATA})\frac{OD^{300}{}_{NATA}}{OD^{300}{}_{PROT}}\frac{\int_{310}^{480}F(\lambda) - R(\lambda)\,d\lambda}{\int_{310}^{480}N(\lambda) - R(\lambda)\,d\lambda}\frac{1}{1+2\bar{r}} \quad (1)$$

where $\bar{r}$ is the steady-state fluorescence anisotropy of the sample, obtained by integration of its polarized fluorescence decays. This correction is justified because the steady-state fluorescence anisotropy of cardiotoxin is approximately constant across its emission spectrum (Mérola et al., unpublished results), while the steady-state anisotropy of NATA is close to zero at room temperature.

Time-Resolved Fluorescence Measurements. The fluorescence decays were measured by the single-photon counting method, using the synchrotron radiation of Super-ACO (LURE, Orsay) as a pulsed excitation source. The optical and electronic parts of the instrumental setup have been described previously (Brochon et al., 1993). The light pulse of Super-ACO, convoluted with the detection response, gave

a mean instrumental function of about 600 ps FWHM, determined with a scattering solution of Ludox (DuPont Co.). The instrumental function, $g(t)$, was recorded at the emission wavelength alternately with the parallel and perpendicular components, $I_{vv}(t)$ and $I_{vh}(t)$, of the fluorescence. The correction factor, β, for the differing sensitivity to polarization was determined from the fluorescence of NATA at 20 °C, measured under the same optical settings:

$$\beta(\lambda_{em}) = \frac{\int_{t_o}^{\infty} I_{vv}(t)\, dt}{\int_{t_o}^{\infty} I_{vh}(t)\, dt} \quad (2)$$

t_o being the time at which the fluorescence of NATA is fully depolarized. Approximately 10–20 million counts were stored in the total fluorescence decay, $I_{vv}(t) + 2\beta I_{vh}(t)$, with each polarized curve being collected over 1024 channels at 35 ps/channel.

The relative level of scattered light present in the fluorescence signal was found to be undetectable (i.e., less than 0.1%), as checked with a Ludox solution observed under the conditions normally used for fluorescence detection. On the other hand, we found that unavoidable changes in optical settings for the respective measurements of fluorescence and instrumental response (such as different positions of the excitation grating) introduced nonnegligible variable optical delays, on the order of 10 ps, between these two functions. The use of a time shift in the analysis greatly improved the quality of the fit at short times, allowing in all cases a satisfactory description of the leading edge of the fluorescence data down to 1% of the peak height. In addition, the introduction of this time shift resulted in much better reproducibility of the recovered lifetime distributions. This time shift was optimized by preliminary least-squares analysis of the data (Grinvald & Steinberg, 1974) and was found to be well-correlated with the changes in optical settings.

Time-Resolved Fluorescence Analysis. Analysis of the fluorescence decays was performed by the maximum entropy method, using the FAME program and MEMSYS2 as library subroutines (MEDC, Ltd). After excitation by a vertically polarized pulse of light, the complete expression of the parallel $I_{vv}(t)$ and perpendicular $\beta I_{vh}(t)$ components of the experimental fluorescence decay are (Livesey & Brochon, 1987)

$$I_{vv}(t) = {}^1/_3 g_\lambda(t) * \int_0^\infty \int_0^\infty \int_{-0.2}^{0.4} \gamma(\tau,\theta,A)\, e^{-t/\tau}(1 + 2Ae^{-t/\theta})\, d\tau\, d\theta\, dA \quad (3)$$

and

$$\beta I_{vh}(t) = {}^1/_3 g_\lambda(t) * \int_0^\infty \int_0^\infty \int_{-0.2}^{0.4} \gamma(\tau,\theta,A)\, e^{-t/\tau}(1 - Ae^{-t/\theta})\, d\tau\, d\theta\, dA \quad (4)$$

where $g_\lambda(t)$ is the measured instrumental function at wavelength λ, * denotes a convolution product, and $\gamma(\tau,\theta,A)$ represents the number of fluorophores with fluorescence lifetime τ, correlation time θ, and initial anisotropy A, assuming that all chromophores have identical absorption coefficients and radiative lifetimes.

Analysis of Total Fluorescence Decays. Analysis of total fluorescence decays by the maximum entropy method has been described in more detail elsewhere (Livesey & Brochon, 1987; Mérola et al., 1989). The total intensity decay is obtained from the parallel and perpendicular components by

$$T(t) = I_{vv}(t) + 2\beta I_{vh}(t) = g_\lambda(t) * \int_0^\infty \alpha(\tau)\, e^{-t/\tau}\, d\tau \quad (5)$$

where $\alpha(\tau)$ is the fluorescence lifetime distribution:

$$\alpha(\tau) = \int_0^\infty \int_{-0.2}^{0.4} \gamma(\tau,\theta,A)\, d\theta\, dA \quad (6)$$

The degree of structure of $\alpha(\tau)$ is quantified by an entropy function, $S(\alpha(\tau))$ (Jaynes, 1983; Livesey & Skilling, 1985). The entropy of $\alpha(\tau)$ is progressively decreased, starting from an initial flat model (Livesey & Brochon, 1987). To ensure that the recovered distribution agrees with the data, this procedure is subjected to the simultaneous constraint of a decrease in reduced χ^2:

$$\chi^2 = \frac{1}{M} \sum_{k=1}^{M} \frac{(T_k^{cal} - T_k^{obs})^2}{\sigma_k^2} \quad (7)$$

where T_k^{cal} and T_k^{obs} are the kth calculated and observed intensities. σ_k^2 is the variance of the kth data point ($\sigma_k^2 = \sigma_{k,vv}^2 + 4\beta^2\sigma_{k,vh}^2$; Wahl, 1979). The expectation value of χ^2 is 1 in the limit of an infinite number of observations M. The distribution $\alpha(\tau)$ is represented by a discrete set, $\alpha(\tau_i)$, of 150 values equally spaced on a logarithmic scale between 5 ps and 12 ns. The analysis is stopped when the fit of the data does not significantly improve, i.e., when $\Delta\chi^2/\chi^2$ over the next 20 iterations is lower than 0.2%, a value that was determined from simulations representative of the cardiotoxin data. This criterion is found to be identical to that used for thioredoxin (Mérola et al., 1989), which probably reflects the similar levels in statistical accuracy and similar complexities of the two inversion problems. In tabulating the results, the center of gravity, $\sum\alpha_i\tau_i$, and the integrated amplitude, $\sum\alpha_i$, of separate peaks in the distribution are used to compute the respective lifetime and fractional amplitude of each principal component. The average fluorescence lifetime, $\bar{\tau}$ is the center of gravity of the overall distribution, after the exclusion of very short unstable amplitudes below 0.05 ns. Errors are estimated from the standard deviation of results from repeated experiments.

Analysis of Fluorescence Anisotropy Decays. The fluorescence anisotropy decays were analyzed using the maximum entropy method under the two following assumptions: (i) All chromophores have the same unknown fundamental anisotropy, $A = r_o$, determined by the angle between absorption and emission moments of the molecule. (ii) The probability, $\varphi_i(\theta)$, for a chromophore i to have a given rotational correlation time θ is independent of its fluorescence lifetime. Hypothesis (i) is reasonable for fluorescence arising only from tryptophan residues excited on the red edge of their absorption band. Hypothesis (ii) is satisfied in two particular situations: first, when all fluorescent species have the same rotational dynamics, and second, when all rotational species have the same fluorescence kinetics. It is thus roughly acceptable in the case of a homogeneous rigid protein showing only small amplitude for nanosecond flexibilities or for proteins having a nearly single-exponential fluorescence kinetics.

In this simplified model, the population distribution, $\gamma(\tau,\theta,A)$, can be written as the product of three independent functions:

$$\gamma(\tau,\theta,A) = \alpha(\tau)\, \varphi(\theta)\, \delta(A) \quad \text{with} \quad \varphi(\theta) = \sum c_i\varphi_i \quad (8)$$

$$\text{and} \left\{ \begin{array}{l} \delta(A) = 1 \quad \text{for} \quad A = r_o \\ \delta(A) = 0 \quad \text{for} \quad A \neq r_o \end{array} \right\}$$

where $\alpha(\tau)$ is the previously determined distribution of

fluorescence lifetimes and $\varphi(\theta)$ is the weighted average distribution of rotational correlation times over all chromophores, with c_i being the fractional concentration of chromophore i. From eqs 6 and 8 it follows that $\varphi(\theta)$ is normalized,

$$\int_0^\infty \varphi(\theta)\, d\theta = 1$$

and the complete expressions eqs 3 and 4 of the polarized components can be rewritten as

$$I_{vv}(t) = {}^1/_3 g_\lambda(t) * ((1 + 2r(t)) \int_0^\infty \alpha(\tau)\, e^{-t/\tau}\, d\tau) \quad (10)$$

$$I_{vh}(t) = {}^1/_3 g_\lambda(t) * ((1 - r(t)) \int_0^\infty \alpha(\tau)\, e^{-t/\tau}\, d\tau) \quad (11)$$

where $r(t)$ is the anisotropy decay of the chromophore mixture for an infinitely short excitation:

$$r(t) = \int_0^\infty \rho(\theta)\, e^{-t/\theta}\, d\theta \quad \text{with} \quad \int_0^\infty \rho(\theta)\, d\theta = \int_0^\infty r_o\, \varphi(\theta)\, d\theta = r_o \quad (12)$$

Another entropy function, independent of τ, may thus characterize the structure of the distribution, $\rho(\theta)$. The distribution $\rho(\theta)$ was represented by a discrete set, $\rho(\theta_i)$, of 100 values equally spaced on a logarithmic scale between 10 ps and 20 ns, plus one channel of a constant anisotropy corresponding to an "infinite" (unmeasurable) correlation time. Analysis was then performed in the same way as for the total fluorescence, the reduced χ^2 being computed on both polarized components, and the fit was arbitrarily stopped at 50 iterations. Given the limited statistics of the data, the distribution $\rho(\theta)$ obtained through the above procedure amounted, in all cases, to the following discrete model:

$$r(t) = r_i(\varphi_c e^{-t/\theta_c} + \varphi_\infty) = r_c e^{-t/\theta_c} + r_\infty \quad (13)$$

r_c and θ_c being the respective amplitude and relaxation time of the time-dependent part of the anisotropy decay, r_∞, is the amplitude of the constant part, and $r_i = r_c + r_\infty$ is the experimental initial anisotropy.

RESULTS

Steady-State Fluorescence at 20 °C. The fluorescence spectra of cardiotoxin, α-neurotoxin, and erabutoxin *b* at 20 °C, pH 7, are shown in Figure 2, for comparison that of *N*-acetyltryptophanamide (NATA). If we assume a fluorescence quantum yield of 14% for NATA (Werner & Fortser, 1979), the approximate quantum yields of the three toxins are, respectively, 5.6%, 9.5%, and 6.8%. The wavelength of maximum emission of all toxins is shifted to the blue as compared to NATA, and the full width at half-maximum values of the spectra are lower than that of NATA (Table 1). Such results are expected for tryptophan residues partially shielded from water (Burstein et al., 1973). The environment of the tryptophan residue appears to be slightly more hydrophobic in the two neurotoxins. The present data are in qualitative agreement with previous intrinsic fluorescence studies on neurotoxins (Nakanishi et al., 1980; Ménez et al., 1980) and cardiotoxins (Vincent et al., 1978; Dufourcq & Faucon, 1978; Gatineau et al., 1987), taking into account differences in excitation wavelengths and monochromator responses.

Fluorescence Decays at 20 °C. Figure 3 shows the experimental fluorescence decays and the residuals from data analysis obtained at 20 °C, pH 7, on the different toxins. The corresponding distributions of fluorescence lifetimes are shown in Figure 4. Cardiotoxin has very complex fluorescence kinetics (Figure 4a), with a large, unresolved profile showing three major components around 0.7 (69%), 2 (28%), and 4.8 ns (3%) (Table 2). The shortest component is probably heterogeneous, and a vanishing shoulder in the short time range is observed in certain cases. These results were found to be roughly insensitive to the selected emission wavelength between 335 and 380 nm (data not shown).

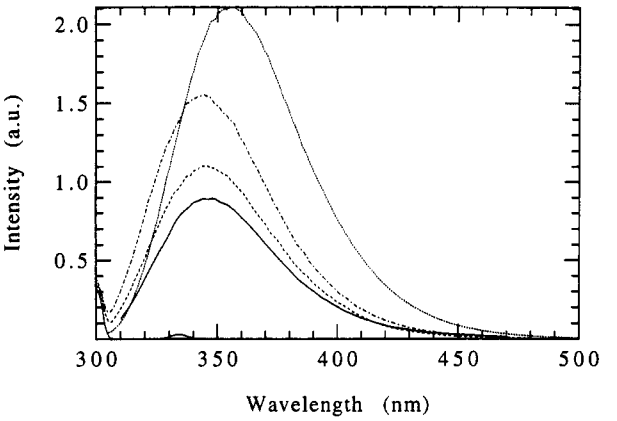

FIGURE 2: Uncorrected tryptophan fluorescence spectra of cardiotoxin and relative buffer signal (—), α-neurotoxin (– · –), erabutoxin *b* (- - -), and *N*-acetyltryptophanamide (···), at 20 °C, pH 7, and λ_{exc} = 300 nm. Intensities have been scaled to the estimated relative quantum yields of the different samples.

The dispersion of the cardiotoxin profiles obtained from repeated experiments at 20 °C (Figure 5) allowed, in all cases, a reproducible separation of the minimum components described above. In addition, the resolution of the different peaks is consistently reduced on cardiotoxin samples contaminated with aggregates (Mérola et al., manuscript in preparation) or denatured forms (see below). The true profile of cardiotoxin fluorescence lifetimes therefore may not be a smooth unimodal broad function (Alcala et al., 1987), which would have been overfit to an artifactual structured solution (James & Ware, 1985).

On the other hand, under identical conditions, least-squares fits of the cardiotoxin decays to three exponential terms systematically yielded higher χ^2 values than the distribution model. The four-exponential solution (Figure 5) corresponds to the splitting of the short component at 0.7 ns between one at 0.3 ns and another at 0.9 ns, with an average χ^2 of 1.34. It was impossible to achieve convergence to a reproducible solution when a fifth exponential term was added. Least-squares fits to a priori discrete exponentials may easily result in arbitrary solutions devoid of physical meaning (James & Ware, 1985). The broad experimental MEM profile therefore must be considered as the best and the most conservative description available today for the cardiotoxin fluorescence kinetics, with a lack of resolution that clearly reflects some underlying complexity.

The two neurotoxins show, on the contrary, very simple and very similar lifetime distributions (Figure 4c,d), dominated in each case by a major peak flanked by two satellites. The major peak represents, respectively, 85% and 79% of the total amplitude for α-neurotoxin and erabutoxin *b*, while the lifetime values are shorter for erabutoxin *b* in keeping with the relative quantum yields of the toxins (Tables 1 and 2). The fluorescence decay of NATA is nearly monoexponential (Figure 4b) with 96% of a 3.07 ± 0.02-ns lifetime, in agreement with our previous determination under laser excitation (Mérola et al., 1989), as well as with literature data on this compound

Table 1: Steady-State Tryptophan Fluorescence, Average Lifetimes, and Radiative Lifetimes[a]

	λ_{max} (nm, ±0.5)	FWHM (nm, ±0.5)	approximate quantum yield (%)	$\bar{\tau}_f$ (ns)[b]	τ_r (ns)
N. nigricollis cardiotoxin	347.7	57.6	5.6 ± 0.6	1.21 ± 0.02	21.6 ± 2
N. nigricollis α-neurotoxin	343.8	57.1	9.5 ± 1.0	1.71 ± 0.04	18.0 ± 2
L. Semifasciata erabutoxin *b*	345.7	57.8	6.8 ± 0.7	1.18 ± 0.02	17.4 ± 2
NATA	355.3	60.8	14.0[c]	3.08[d]	21.9

[a] 20 °C, pH 7, λ_{exc} = 300 nm, and $\Delta\lambda_{exc} = \lambda_{em}$ = 4 nm. [b] Computed from Table 2. [c] From Werner and Forster (1979), taken as reference. [d] From Mérola et al. (1989) and Table 2.

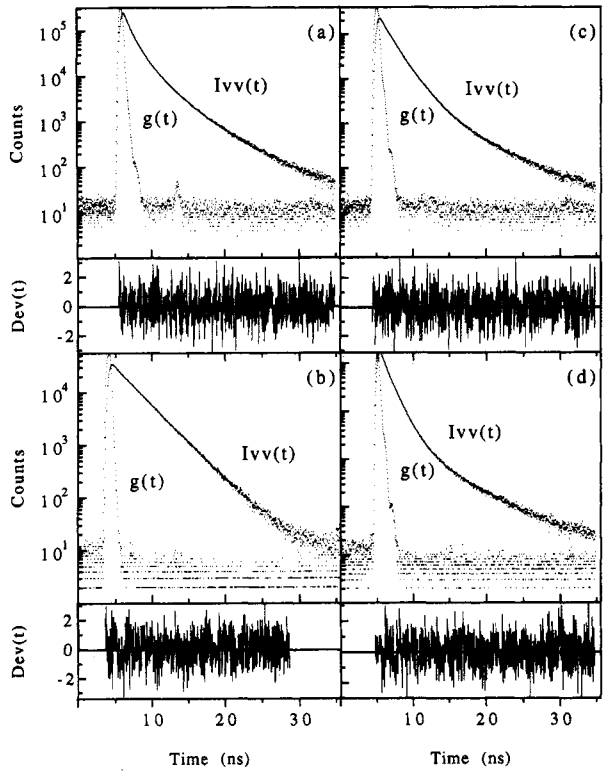

FIGURE 3: Experimental fluorescence decays of (a) cardiotoxin, (b) *N*-acetyltryptophanamide, (c) α-neurotoxin, and (d) erabutoxin *b* at 20 °C, λ_{exc} = 300 nm, and λ_{em} = 347 nm. $I_w(t)$, parallel component of the decay; $g(t)$, instrumental function; Dev(t), residual after maximum entropy analysis.

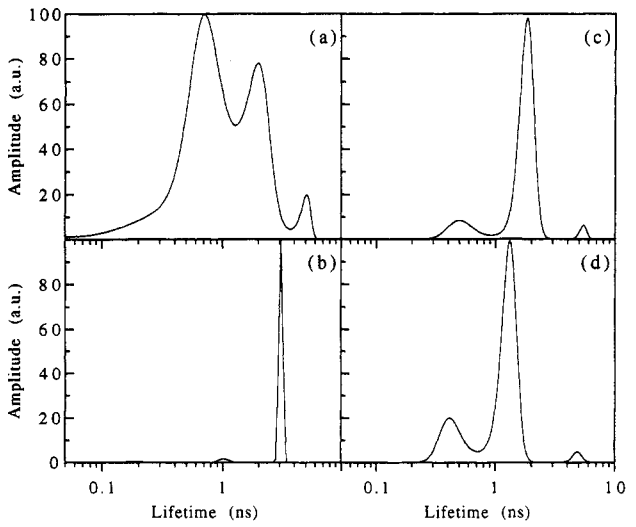

FIGURE 4: Distribution of fluorescence lifetimes of (a) Trp11 of cardiotoxin, (b) *N*-acetyltryptophanamide, (c) Trp29 of α-neurotoxin, and (d) Trp29 of erabutoxin *b*, as recovered by maximum entropy analysis of the corresponding decays of Figure 3a–d.

(Szabo & Rayner, 1980; Willis & Szabo, 1992). The 4% short component would require further investigation to determine whether it is a proper kinetic term of NATA rather than some contamination or artifact.

Table 2: Principal Components of the Fluorescence Decays[a]

	lifetimes (ns, top) and amplitudes (%, bottom)			χ^2
N. nigricollis cardiotoxin	0.71 ± 0.04 69 ± 3	2.05 ± 0.08 28 ± 3	4.8 ± 0.1 3 ± 1	1.18
N. nigricollis α-neurotoxin	0.49 ± 0.06 13 ± 1	1.78 ± 0.02 85 ± 1	5.2 ± 0.1 3 ± 1	1.02
L. semifasciata erabutoxin *b*	0.42 ± 0.06 19 ± 3	1.26 ± 0.02 79 ± 3	4.8 ± 0.1 2 ± 1	1.00
NATA		1.07 ± 0.05 4 ± 1	3.07 ± 0.02 96 ± 1	1.05

[a] 20 °C, pH 7, λ_{exc} = 300 nm, λ_{em} = 347 nm, and $\Delta\lambda_{exc} = \Delta\lambda_{em}$ = 6 nm.

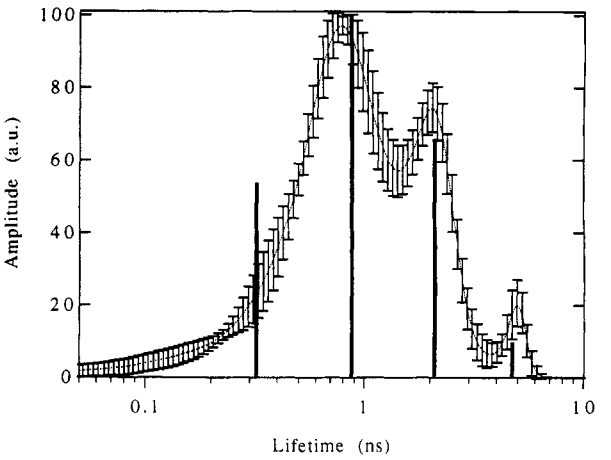

FIGURE 5: Average fluorescence lifetime distribution of cardiotoxin Trp11, standard deviation over repeated experiments at 20 °C (five determinations), and (bars) average solution of least-squares fits of the same data to four discrete exponential terms.

Apparent Radiative Lifetimes. The determination of both fluorescence lifetimes and quantum yields allows an estimate of the radiative lifetime, τ_r, of tryptophan in the different proteins (De Lauder & Wahl, 1970), in comparison with that of the free compound. Stable ground-state interactions within the protein matrix, leading to static quenching, will dramatically increase the apparent value of the radiative lifetime due to the existence of a nonfluorescent, although absorbing, population of tryptophan residues. Perturbations of the electronic structure of tryptophan may also result in small changes in its intrinsic radiative lifetime. For NATA, our time-resolved measurements yield a radiative lifetime of 21.9 ns, which is in good agreement with literature values (Ricci, 1970; Szabo & Rayner, 1980; Chen et al., 1991). The radiative lifetimes of cardiotoxin, α-neurotoxin, and erabutoxin *b* at 20 °C are found to equal 21.6, 18.0, and 17.4 ns, respectively (Table 1). On the one hand, these low values indicate, in all cases, the absence of large amounts of static quenching. On the other hand, the neurotoxins exhibit a somewhat decreased value, similar to that observed for aqueous tryptophan at high pH (Chang et al., 1983), which may indicate a specific perturbation of the chromophore in these proteins.

Fluorescence Anisotropy Decays at 20 °C. The fluorescence anisotropy decays of all highly purified toxins at 20 °C are

Table 3: Parameters of the Fluorescence Anisotropy Decays[a]

	r_i (±0.006)	θ_c (ns, ±0.2)	r_∞/r_i (%)	$\bar{r}$ (±0.004)	χ^2
N. nigricollis cardiotoxin	0.263	3.6	0	0.180	1.12
N. nigricollis α-neurotoxin	0.282	3.7	0	0.188	1.03
L. Semifasciata erabutoxin *b*	0.279	3.6	0	0.205	1.03

[a] All experimental conditions the same as in Table 2.

well-described by single-exponential functions having about the same relaxation time (Table 3). Contrary to cardiotoxin, no detectable aggregation has ever been observed for both neurotoxins. This simple anisotropy decay indicates the absence of large segmental flexibilities in all cases. Its relaxation time should thus mostly reflect the overall tumbling of the toxins, but may be averaged to some extent with unseparated terms corresponding to limited independent motions of the tryptophan residue.

The correlation time for the rotational diffusion of a rigid spherical protein of MW 6800 in water at 20 °C may be computed from the Einstein–Stokes relation. To the dry volume of the protein (0.73 mL/g) must be added about 75% of an additional hydration volume to fit experimental observations on small proteins (Wahl, 1980; Kouyama et al., 1989). Under this spherical model, the time of rotation of cardiotoxin and neurotoxins would be on the order of 3.5 ns, which is very close to measured values.

However, the overall shape of the toxins is rather that of an oblate ellipsoid. In this case, the different locations of the tryptophan residue in cardiotoxin and in neurotoxin could give rise to different apparent rotational correlation times. The maximum dimensions of cardiotoxin and neurotoxin are about the same: 38 × 32 × 21 Å on the average for cardiotoxin (Rees et al., 1990; Gilquin et al., 1993) and 39 × 32 × 21 Å for erabutoxin *b* (Bourne et al., 1985). In addition, the orientation of the tryptophan indole ring happens to be very similar in cardiotoxin and erabutoxin, the ^1L_a absorption dipole making, in both cases, an approximately 70 °C angle with the symmetry axis of the equivalent ellipsoid. As a consequence, we found that the apparent harmonic correlation times of the dry proteins should not differ by more than about 10% (Ehrenberg & Rigler, 1972). This result was insensitive to several alternative assumptions made concerning the orientation of the emission dipole (Ichiye & Karplus, 1983). The similar experimental values of θ_c obtained for cardiotoxin and neurotoxins thus mostly reflect the similar size and shape of fairly rigid proteins.

Nevertheless, the initial anisotropies of the decays show significant differences between the two types of toxins (Table 3). The maximum anisotropy of tryptophan fluorescence in solution, linked to the relative orientation of absorption and emission dipoles in the chromophore, should not exceed 0.30 in the absence of any depolarization process for excitation at 300 nm (Valeur & Weber, 1977). A significantly lower value is observed in cardiotoxin, which probably results from the fast rotational dynamics of the tryptophan side chain below the ultimate time resolution of our data (about 100 ps). The initial anisotropy of the two neurotoxins is higher and is identical for the two toxins, showing that the tryptophan has more restricted rotational freedom in this case.

Cardiotoxin Fluorescence as a Function of Temperature. Like most venom toxins, cardiotoxin is a highly thermostable protein: by steady-state anisotropy measurements, we have determined a local denaturation temperature around Trp11

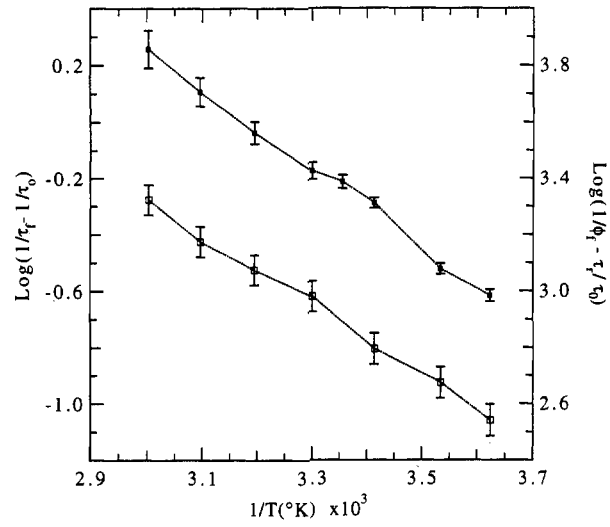

FIGURE 6: Arrhenius plots of (□) fluorescence quantum yield ϕ_f and (■) average fluorescence lifetime $\bar{\tau}_f$ of the cardiotoxin tryptophan from 3 to 60 °C.

of 77 ± 5 °C (Mérola et al., unpublished results). From 3 to 60 °C, the ratio of the quantum yield to the fluorescence lifetime of cardiotoxin remains constant (Figure 6), which confirms the absence of static quenching, expected to decrease with temperature (Swadesh et al., 1987; Mérola et al., 1989). The average radiative rate, $k_r = \phi_f/\bar{\tau}_f = (4.4 \pm 0.2) \times 10^7$ s^{-1}, from 3 to 60 °C is in excellent agreement with the approximate value of 4.5×10^7 s^{-1} determined for many aqueous derivatives of tryptophan (Ricci, 1970; Kirby & Steiner, 1970; Robbins et al., 1980). Simultaneously, the shape and position of the steady-state emission of cardiotoxin remain unchanged over this large temperature range (data not shown).

The fluorescence lifetime distributions of cardiotoxin as a function of temperature are shown in Figure 7. Globally, they show the expected effects of thermal quenching, i.e., a speeding up of all activated quenching processes, resulting in a general decrease in excited-state lifetimes (shifts in peak positions) and, thus, in fluorescence intensity. However, temperature also induces a remarkable redistribution in lifetime populations. Between 3 and 30 °C, the profile remains approximately constant (considering the instability in recovering the shoulder in the short time range). The distribution begins to reorganize above 30 °C with the central components merging together, resulting at 60 °C in a profile dominated by a single peak at 0.6 ± 0.2 ns. The longest lifetime remains well-separated from the rest of the distribution up to 60 °C, while its relative weight increases slightly from 3% to 7%. This reorganization of the cardiotoxin fluorescence lifetime distribution with temperature shows that its different components are under mutual exchange. The interconversion rates, being on a slow or intermediate nanosecond time scale below 20 °C, would become sufficiently fast above 30 °C to merge some components into apparent averages, resulting in a simplification of the profile at high temperatures.

Arrhenius Behavior of Fluorescence Lifetimes. The average fluorescence lifetime of cardiotoxin significantly deviates from a simple Arrhenius law, while inaccuracies forbid the parallel detection of this small deviation from steady-state data (Figure 6). Such complex behavior is not really surprising for a highly heterogeneous fluorescence undergoing important redistributions with temperature. Figure 8 shows the tentative Arrhenius plots of individual fluorescence lifetimes, wherever they could be separated in the distributions (Figure 7). These components show significantly different temperature respons-

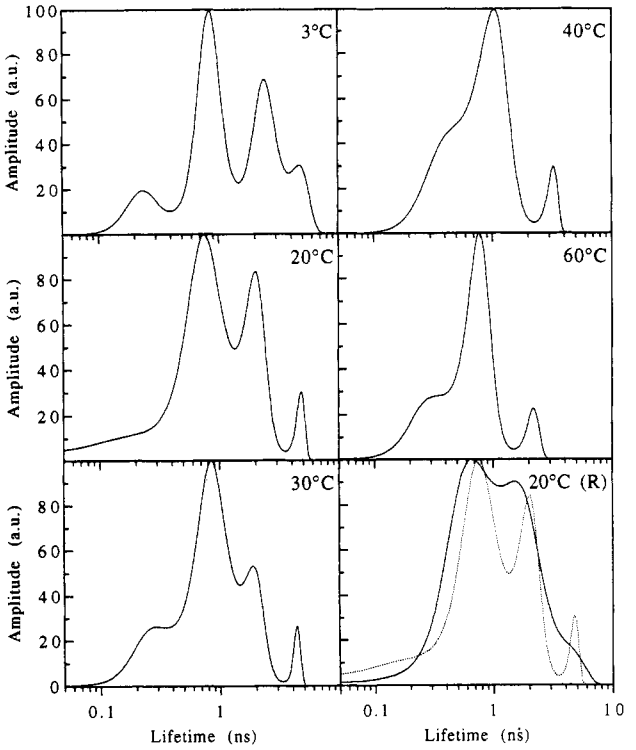

FIGURE 7: Temperature dependence of the distribution of cardiotoxin fluorescence lifetimes. (R): Reversibility at 20 °C after the complete temperature study, including 2 h at 60 °C, compared with (···) unheated cardiotoxin at 20 °C.

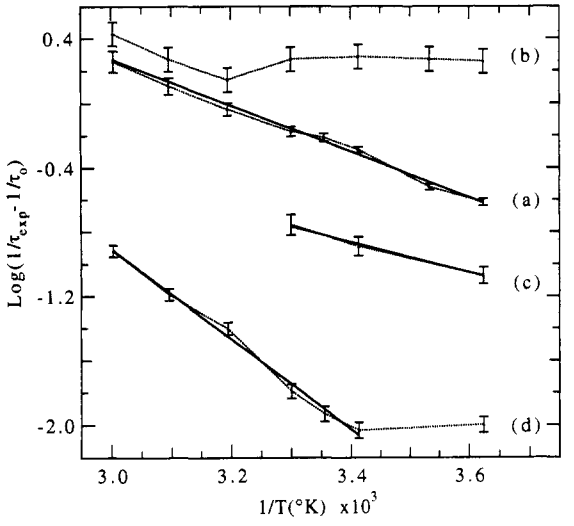

FIGURE 8: Arrhenius plots of the principal fluorescence lifetimes of cardiotoxin as separated in the distributions of Figure 7: (a) average fluorescence lifetime $\bar{\tau}_f$; (b) average of all components below 1 ns; (c) intermediate component, which merges into b above 30 °C; and (d) long component, which is not completely separated from the intermediate one below 20 °C. $\tau_o = 1/k_r + k_{isc}$ is computed from experimental and literature data as described in the text. Continuous lines are linear fits to $\ln(A) - E_a/RT$, where A is the frequency factor, E_a is the activation energy, R is the gas constant, and T is the absolute temperature: (a) $A = 10^{11}$ s^{-1}, $E_a = 2.9 \pm 0.1$ kcal/mol, correlation coefficient = 0.997; (b) not fitted; (c) $A = 10^{10}$ s^{-1}, $E_a = 1.9 \pm 0.5$ kcal/mol; (d) $A = 2 \times 10^{12}$ s^{-1}, $E_a = 5.6 \pm 0.3$ kcal/mol.

es. The shortest component (taken as the average of the two components below 1 ns) shows almost no temperature dependency up to 30 °C. Above this temperature, it includes the contribution of the intermediate component, which has merged into it (Figure 7). This is reflected by the sudden break in the position and slope of the Arrhenius plot. The longest lifetime is well-separated from the other components at all temperatures above 20 °C and could correspond to a

Table 4: Fluorescence Anisotropy Decays of *N. nigricollis* Cardiotoxin vs Temperature[a]

temp (°C)	r_i (±0.006)	θ_c (ns, ±4%)	r_∞/r_i (%)	$\bar{r}$ (±0.004)	χ^2
3	0.284	7.0	0	0.209	1.12
10	0.275	5.1	1	0.196	1.13
20	0.263	3.6	0	0.180	1.12
25	0.260	3.0	0	0.173	1.17
30	0.261	2.6	1	0.171	1.14
40	0.250	2.1	1	0.159	1.14
50	0.244	1.6	1	0.151	1.10
60	0.235	1.3	2	0.145	1.17
20 (R)[b]	0.257	3.6	0	0.175	1.16

[a] Other experimental conditions are given in Table 2. [b] Reversibility after the complete experiment (12 h), including 2 h at 60 °C.

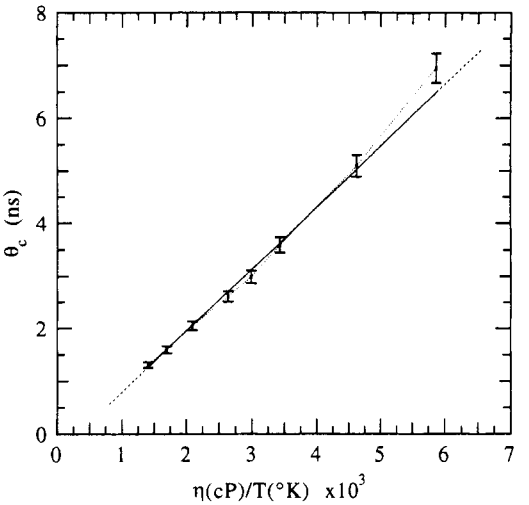

FIGURE 9: Apparent rotational correlation time, θ_c, of cardiotoxin vs η/T: (■) experimental data from Table 4; (—) linear fit to $C + \eta V/kT$, k being the Boltzmann constant; and (- - -) extrapolation of the fit (linear correlation coefficient $r = 0.996$). Partial linear fits to the same function: $r = 0.9993$ from 3 to 25 °C and $r = 0.9997$ from 30 to 60 °C. [The viscosity of water was taken from *CRC Handbook of Chemistry & Physics*, 70th ed., CRC Press, Boca Raton, FL.]

relatively stable species on the nanosecond time scale. An Arrhenius fit of this component yields an activation energy of 5.6 ± 0.3 kcal/mol and a frequency factor of (2 ± 1) × 10^{12} s^{-1} under a linear fit, assuming the same intersystem crossing rate, $k_{isc} = 3.3 \times 10^7$ s^{-1}, as for aqueous tryptophan (Robbins et al., 1980). An exponential fit without a priori assumptions gave the same results within large error bars.

Cardiotoxin Fluorescence Anisotropy as a Function of Temperature. The fluorescence anisotropy decays of cardiotoxin are well-represented at all temperatures by a single-exponential term (Table 4). The decrease in the initial anisotropy indicates an increase in the rate and/or the amplitude of the very fast flexibilities with temperature, which is expected in a diffusive model of these depolarizations. The nanosecond relaxation time, θ_c, of the decay is plotted in Figure 9 as a function of η/T. If one takes all data points in a linear fit, the slope obtained corresponds to an apparent hydration rate of 96%, the fit being nearly acceptable in the extreme limits of some error bars. However, the line does not cross the axes at the origin, as it should do if θ_c simply followed an Einstein–Stokes relation. In fact, the data show a slight upward curvature with a break around 30 °C. A linear fit of the high-temperature points results in an apparent hydration of 78%, while it becomes 130% in the low-temperature range with, in both cases, better quality for these partial fits.

This curvature can be explained if one assumes that some limited nanosecond flexibilities are present, with the amplitude

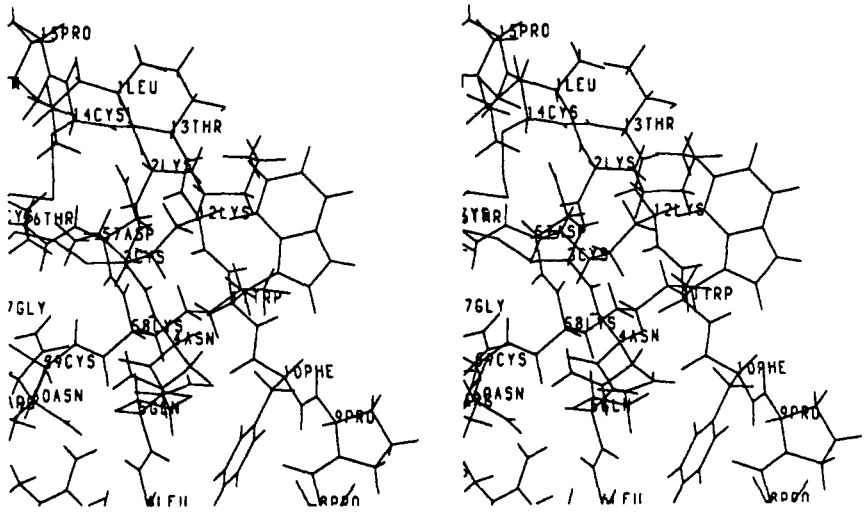

FIGURE 10: Local environment of Trp11 in loop I of *N. nigricollis*. cardiotoxin, according to the NMR solution structure of Gilquin et al. (1993) (stereoview).

or time constant insufficient to give rise to separable terms in the experimental anisotropy decays. In this case, the apparent relaxation time of the anisotropy decay is some weighted average between the correlation times of the overall tumbling and the flexibility. If, in addition, the relative contribution of the flexibility to the depolarization increases with temperature, this will result in nonlinear Perrin plots. A similar effect could also be observed if, for any reason, the apparent hydrodynamic volume of the protein changed with temperature: a change in hydration or in the average orientation of the indole moiety relative to the principal axes of the protein. However, the tryptophan orientation should have limited effects, since cardiotoxin is not sufficiently asymmetric to give rise to very different orthogonal correlation times.

Reversibility of the Temperature Effects on Cardiotoxin. The fluorescence lifetime distribution of heated cardiotoxin at 20 °C after the complete experiment, including 2 h at 60 °C, is strongly perturbed: it is now a broad envelope with almost no structure, although it is approximately centered around the distribution of the intact native protein (Figure 7). No apparent evolution of this profile toward reversibility was observed after 12 h. As was also found in the case of partly aggregated cardiotoxin samples (Mérola et al., manuscript in preparation), relatively small amounts of contaminant may rapidly blur the resolution of a fluorescence lifetime distribution. In the present case, this would arise from some irreversibly denatured forms induced by the heating of cardiotoxin, even though we restricted our study to temperatures below the denaturation transition. The anisotropy decays of heated cardiotoxin give, however, a single rotational correlation time and an initial anisotropy that are both very similar to those of the native protein, with no significant aggregation as seen from the amplitude of the infinite term (Table 4). Completely denatured proteins usually show a strongly decreased initial anisotropy and multiple relaxation terms down to the sub-nanosecond range (Eftink et al., 1991; Chabbert et al., 1992), corresponding to complex segmental flexibilities. Therefore, the denatured forms in heated cardiotoxin either have a very small contribution to the total fluorescence signal or still correspond to relatively globular, compact forms.

DISCUSSION

From an examination of their steady-state fluorescence and their anisotropy decays, the tryptophan residues of all three toxins studied in this article appear to be partly shielded from water and relatively blocked in the protein matrix. The high initial amplitude and the absence of a separable sub-nanosecond relaxation time in the fluorescence anisotropy decays place these proteins among the most rigid ones (Kouyama et al., 1989; Lakowicz et al., 1991).

While proteins tend to display mostly similar steady-state fluorescence spectra, they clearly can exhibit very different time-resolved patterns, ranging from the extreme complexity of the fluorescence lifetime distribution of cardiotoxin at 20 °C to nearly pure single-exponential kinetics like those of neurotoxins. As exemplified in the present and previous studies, each of these patterns appears highly typical of a given protein in a given physical and chemical state. In a sense, the distribution of intrinsic fluorescence lifetimes of a protein is an accurate and specific spectroscopic signature.

Examples of the complex intrinsic fluorescence of single tryptophan residues in proteins are numerous (Beechem & Brand, 1985; Prendergast, 1991), while nearly single exponentials were also found in some cases, such as ribonuclease T1 (James et al., 1985), apoazurin (Hutnik & Szabo, 1989), dendrotoxin (Hollecker et al., 1992), or human recombinant interferon (Brochon et al., 1993). The broad, unresolved profile observed for cardiotoxin is, however, unique among the few proteins studied up to now by the recent method of recovery of fluorescence lifetime distributions (Livesey & Brochon, 1987; Alcala et al., 1987; Lakowicz et al., 1987; Siemiarczuk et al., 1990). This highly heterogeneous fluorescence signal may arise from two possibly simultaneous causes: (i) the coexistence of a large number of discrete, stable microenvironments on the nanosecond time scale, possibly combined with a lack of experimental resolution of these discrete species; (ii) a nonexponential decay law for fluorescence kinetics in this protein (Alcala et al., 1987; Lakowicz et al., 1987; Tanaka & Mataga, 1987). A complete model will have to account not only for the width of the cardiotoxin lifetime distribution but also for its stable substructures, their internal exchanges, and differential temperature dependencies.

A large number of configurations of Trp11 may be allowed by its relatively external, unhindered location in cardiotoxin (Figure 10). If some of these configurations are generated by the intrinsic mobility of the tryptophan side chain on the nanosecond or sub-nanosecond time scale, this should be reflected in its fluorescence anisotropy decays. Picosecond motions, as detected from the low value of the initial fluorescence anisotropy, are in principle too fast to induce

fluorescence heterogeneities directly. On longer time scales, the temperature dependence of the cardiotoxin rotational correlation time suggests limited nanosecond flexibilities, which would increase above 30 °C. These flexibilities could be correlated with the redistributions in fluorescence lifetimes, which also seem to be triggered between 30 and 40 °C. On the other hand, conformational fluctuations of neighboring side chains could further increase the complexity of the fluorescence in a combinatory way, without contributing to the depolarization. The best candidates would be Lys2 and Lys58, which also contain two relatively unhindered external side chains and are the only polar residues in the vicinity. Lys2 has its ammonium group less than 6 Å away from the indole ring in the NMR structure (Gilquin et al., 1993). In pH studies (Blandin, 1990), the fluorescence signal of Trp11 was found to be very sensitive to the neutralization of a lysine residue.

Due to the intrinsic limitations of time-resolved experiments, the resolution of a fluorescence lifetime distribution will quickly collapse when more than a few discrete components are present (Alcala et al., 1987; Mérola et al., 1989; Royer, 1992; Siemiarczuk et al., 1990). Therefore, a combinatory model of a few discrete side-chain rotamers under nanosecond or slower equilibrium, each combination being associated with a single-exponential fluorescence decay, would appear sufficient to rationalize, in a simple and consistent way, the complex cardiotoxin fluorescence kinetics together with its temperature responses and anisotropy decays. This does not presume anything concerning the pertinence of nonexponential kinetic models arising from transient effects in dynamic quenching or dielectric relaxation on the nanosecond time scale (Ware, 1980; Lakowicz et al., 1987), which would be, however, very difficult to demonstrate as such in the present case.

The components of cardiotoxin fluorescence show a wide range of Arrhenius dependencies. These different responses suggest that each species undergoes a different dominant process of desexcitation, governed by a different activation barrier. However, when fluorescent states are under intermediate nanosecond exchange, the apparent fluorescence lifetimes will be strongly affected by the variations in their interconversion rates (Donzel et al., 1974). In this case, the slopes of the Arrhenius plots have little to do with the activation energies of fluorescence quenching processes. However, when an apparently pure fluorescence lifetime (i.e., presumably exchanging on slow time scales) could be separated in the very complex cardiotoxin fluorescence, its energetic parameters fell in the range observed for many derivatives of tryptophan in solution (Robbins et al., 1980; Petrich et al., 1983), which suggests a similar dominant mechanism of desexcitation in this case.

Trp11 belongs to the most external strand of the small β-sheet of loop I in cardiotoxin. Relatively high temperature factors were observed in this region, together with the tip of loop II, in the crystal structure of *Naja mossambica mossambica* cardiotoxin V^{II}_4 (Rees et al., 1990). A specific flexibility of loop I in cardiotoxin has also been suggested from NMR solution studies (Steinmetz et al., 1988). In the interaction of cardiotoxin with model membranes (Dufourcq et al., 1982), loop I has been shown to embed in the hydrophobic core, and the perturbations of the lipids have been ascribed to a subsequent wedge action of the protein inside the bilayer. These hydrophobic interactions might imply significant conformational rearrangements, for which potential flexibilities of the aqueous toxin would be required.

Early comparative NMR studies have suggested that neurotoxins are markedly more rigid than cardiotoxins and stressed that the spatial environment of Trp29 is highly conserved between neurotoxins from different species (Lauterwein et al., 1978). Trp29 is hydrogen-bonded through a water molecule to Asp31 and shows low temperature factors in erabutoxin *b* (Low & Corfield, 1986), while it has a unique χ_1 rotamer in α-neurotoxin (Zinn-Justin et al., 1992). It is the central residue of a compact cluster, which shows delayed denaturation (Endo & Tamiya, 1991). The fluorescence decays of the neurotoxins confirm the nearly unique structure, at all time scales above the sub-nanosecond range, in the vicinity of this tryptophan residue. The high initial anisotropy shows that the dynamics in the very fast time range is also strongly limited, although not completely absent. This very rigid picture contrasts with the conclusions drawn by Tanaka and co-workers (Tanaka et al., 1987) from the application of their model of nonexponential fluorescence kinetics to erabutoxin *b*. Temperature studies are under way to further characterize the kinetic processes in this protein.

Although erabutoxin *b* and α-neurotoxin have only 70% homology in amino acid sequence, they show striking similarities in the fluorescence of their single tryptophan residue. The only notable difference between the two proteins is the relatively lower fluorescence intensity of erabutoxin *b*. Such a difference may easily be caused by a single additional or more efficient quenching process within an otherwise identical microenvironment. In the β-sheet of loop II, the side chains that can interact with Trp29, at a distance of two residues, are the same in both sequences, while the residues that differ are, on the contrary, oriented away from the tryptophan. The identical fluorescence lifetime profiles show that not only the precise electronic environment of the tryptophan residue but also its dynamic fluctuations are conserved in both proteins, which probably reflects the importance of this area for interaction of the toxin with the acetylcholine receptor (Low & Corfield, 1986; Chatrenet et al., 1990).

ACKNOWLEDGMENT

We are grateful to B. Gilquin, C. Roumestand, and F. Toma for communicating the NMR solution coordinates of *Naja nigricollis* cardiotoxin before publication and for fruitful discussions. We thank the technical staff of LURE for running the synchrotron machine and computing facilities. Molecular graphics were prepared using an academic version of MANOSK kindly supplied by the authors (Cherfils et al., 1988).

REFERENCES

Alcala, J. R., Gratton, E., & Prendergast, F. G. (1987) *Biophys. J. 51*, 587–596, 597–604, and 925–936.

Beechem, J. M., & Brand, L. (1985) *Annu. Rev. Biochem. 54*, 43–71.

Blandin, P. (1990) *Rapport de stage de DEA*, Paris XI, Orsay.

Bougis, P. E., Tessier, M., Van Rietschoten, J., Rochat, H., Faucon, J. F., & Dufourcq, J. (1983) *Mol. Cell. Biochem. 55*, 49–64.

Bougis, P. E., Marchot, P., & Rochat, H. (1986) *Biochemistry 25*, 7235–7243.

Bourne, P. E., Sato, A., Corfield, P. W. R., Rosen, L. S., Birken, S., & Low, B. L. (1985) *Eur. J. Biochem. 153*, 521–527.

Brochon, J. C., Tauc, P., Mérola, F., & Schoot, B. M. (1993) *Anal. Chem. 65*, 1028–1034.

Burstein, E. A., Vedenkina, N. S., & Ivkova, M. N. (1973) *Photochem. Photobiol. 18*, 263–279.

Chabbert, M., Hillen, W., Hansen, D., Takahashi M., & Bousquet, J. A. (1992) *Biochemistry 31*, 1951–1960.

Chang, M. C., Petrich, J. W., McDonald, D. B., & Fleming, G. R. (1983) *J. Am. Chem. Soc. 105*, 3819–3824.
Chatrenet, B., Trémeau, O., Bontems, F., Goeldner, M. P., Hirth, C. G., & Ménez, A. (1990) *Proc. Natl. Acad. Sci. U.S.A. 87*, 3378–3382.
Chen, R. F., Knutson, J. R., Ziffer, H., & Porter, D. (1991) *Biochemistry 30*, 5184–5195.
Cherfils, J., Vaney, M. C., Morize, I., Surcouf, E., Colloc'h, N., & Mornon, J. P. (1988) *J. Mol. Graphics 6*, 155–160.
De Lauder, W. B., & Wahl, P. (1970) *Biochemistry 9*, 2750–2754.
Désormeaux, A., Laroche, G., Bougis, P. E., & Pézolet, M. (1992) *Biochemistry 31*, 12173–12182.
Donzel, B., Gauduchon, P., & Wahl, P. (1974) *J. Am. Chem. Soc. 96*, 801–808.
Dufourcq, J., & Faucon, J. F. (1978) *Biochemistry 17*, 1170–1176.
Dufourcq, J., Faucon, J. F., Bernard, E., & Pezolet, M. (1982) *Toxicon 20*, 165–174.
Dufton, M. J., & Hider, R. C. (1988) *Pharmacol. Ther. 36*, 1–40.
Eftink, M. R., Gryczynski, I., Wiczk, W., Laczko, G., & Lakowicz, J. R. (1991) *Biochemistry 30*, 8945–8953.
Ehrenberg, M., & Rigler, R. (1972) *Chem. Phys. Lett. 14* 539–544.
Endo, T., & Tamiya, N. (1991) in *Snake Toxins* (Harvey, A. L., Ed.) pp 165–222, Pergamon Press, New York.
Fryklund, L., & Eacker, D. (1975) *Biochemistry 14*, 2865–2871.
Gatineau, E., Toma, F., Montenay-Garestier, T., Takechi, M., Fromageot, P., & Ménez, A. (1987) *Biochemistry 26*, 8046–8055.
Gatineau, E., Takechi, M., Bouet, F., Mansuelle, P., Rochat, H., Harvey, A. L., Montenay-Garestier, T., & Ménez, A. (1990) *Biochemistry 29*, 6480–6489.
Gilquin, B., Roumestand, C., Zinn-Justin, S., Ménez, A., & Toma, F. (1993) *Biopolymers 33*, 1659–1675.
Grinvald, E., & Steinberg, I. Z. (1974) *Anal. Biochem. 59*, 583–598.
Grognet, J. M. (1988) Thèse de 3ème Cycle, Paris V, France.
Hollecker, M., Tauc, P., & Brochon, J. C. (1992) XIth Colloque Annuel de la Société Française de Biophysique, Orléans, France, September 15–17, 1992.
Hutnik, C. M., & Szabo, A. G. (1989) *Biochemistry 28*, 3935–3939.
Ichiye, T., & Karplus, M. (1983) *Biochemistry 22*, 2884–2894.
James, D. R., & Ware, W. R. (1985) *Chem. Phys. Lett. 120*, 455–459.
James, D. R., Demmer, D. R., Steer, R. P., & Verrall, R. E. (1985) *Biochemistry 24*, 5517–5526.
Jaynes, E. T. (1983) in *Collected Works, Papers on Probability Statistics and Statistical Physics* (Rosenkrantz, R. D., Ed.) D. Reidel, Dordrecht, The Netherlands.
Kirby, E. P., & Steiner, R. F. (1970) *J. Phys. Chem. 74*, 4480–4490.
Kouyama, T., Kinosita, K., & Ikegami A. (1989) *Eur. J. Biochem. 182*, 517–512.
Lakowicz, J. R., Cherek, H., Gryczynski, I., Joshi, N., & Johnson, M. L. (1987) *Biophys. Chem. 28*, 35–50.
Lakowicz, J. R., Gryczynski, I., Szmacinski, H., Cherek, H., & Joshi, N. (1991) *Eur. Biophys. J. 19*, 125–140.
Lauterwein, J., Lazdunski, M., & Wüthrich, K. (1978) *Eur. J. Biochem. 92*, 361–371.
Livesey, A. K., & Skilling, J. (1985) *Acta Crystallogr. A41*, 113–122.
Livesey, A. K., & Brochon, J. C. (1987) *Biophys. J. 52*, 693–706.
Low, B. W., & Corfield, W. R. (1986) *Eur. J. Biochem. 161*, 579–587.
Marchot, P., Bougis, P. E., Ceard, B., Van Rietschoten, J., & Rochat, H. (1988) *Biochem. Biophys. Res. Commun. 153*, 642–647.
Ménez, A., Montenay-Garestier, T., Fromageot, P., & Hélène C. (1980) *Biochemistry 19*, 5202–5208.
Ménez, A., Gatineau, E., Roumestand, C., Harvey, A. L., Mouawad, L., Gilquin, B., & Toma, F. (1990) *Biochimie 72*, 575–588.
Mérola, F., Rigler, R., Holmgren, A., & Brochon, J. C. (1989) *Biochemistry 28*, 3383–3398.
Nakanishi, M., Kobayashi, M., Tsuboi, M., Takasaki, C., & Tamiya, N. (1980) *Biochemistry 19*, 3204–3208.
Petrich, J. W., Chang, M. C., McDonald, D. B., & Fleming G. R. (1983) *J. Am. Chem. Soc. 105*, 3824–3832.
Prendergast, F. G. (1991) *Curr. Opin. Struct. Biol. 1*, 1054–1059.
Rees, B., Samama, J. P., Thierry, J. C., Gilibert, M., Fischer, J., Schweitz, H., & Lazdunski, M. (1987) *Proc. Nat. Acad. Sci. U.S.A. 84*, 3132–3136.
Rees, B., Bilwes, A., Samama, J. P., & Moras, D. (1990) *J. Mol. Biol. 214*, 281–297.
Ricci, R. W. (1970) *Photochem. Photobiol. 12*, 67–75.
Robbins, R. J., Fleming, G. R., Beddard, G. S., Robinson, G. W., Thistlethwaite, P. J., & Woolfe, G. J. (1980) *J. Am. Chem. Soc. 102*, 6271–6279
Royer, C. A. (1992) *Biophys. J. 63*, 741–750.
Siemiarczuk, A., Wagner, B. D., & Ware, W. R. (1990) *J. Phys. Chem. 94*, 1661–1666.
Steinmetz, W. E., Bougis, P. E., Rochat, H., Redwine, O. D., Braun, W., & Wüthrich, K. (1988) *Eur. J. Biochem. 172*, 101–116.
Swadesh, J. K., Mui, P. W., & Sheraga, H. A. (1987) *Biochemistry 26*, 5761–5769.
Szabo, A. G., & Rayner, D. M. (1980) *J. Am. Chem. Soc. 102* 554–563.
Tanaka, F., & Mataga, N. (1987) *Biophys. J. 51*, 487–495.
Tanaka, F., Kaneda, N., Mataga, N., Tamai, N., Yamazaki, I., & Hayashi, K. (1987) *J. Phys. Chem. 91*, 6344–6346.
Valeur, B., & Weber, G. (1977) *Photochem. Photobiol. 25*, 441–444.
Vincent, J. P., Balerna, M., & Lazdunski, M. (1978) *FEBS Lett. 85*, 103–108.
Wahl, P. (1979) *Biophys. Chem. 10*, 91–104.
Wahl, P. (1980) in *Time resolved spectroscopy in biochemistry and biology* (Cundall, R. B., & Dale, R. E., Eds.) pp 497–521, Plenum Press, New York.
Ware, W. R. (1980) in *Time resolved spectroscopy in biochemistry and biology* (Cundall, R. B., & Dale, R. E., Eds.) pp 299–317, Plenum Press, New York.
Werner, T. C., & Forster, L. S. (1979) *Photochem. Photobiol. 29*, 905–914.
Willis, K. J., & Szabo, A. G. (1992) *Biochemistry 31*, 8924–8931.
Zinn-Justin, S., Roumestand, C., Gilquin, B., Bontems, F., Ménez, A., & Toma, F. (1992) *Biochemistry 31*, 11335–11347.